Impulse Sensitivity Function Analysis of Periodic Circuits

Jaeha Kim, Brian S. Leibowitz, Metha Jeeradit
Rambus, Inc., 4440 El Camino Real, Los Altos, CA 94022, USA

ABSTRACT
This paper describes an efficient method to characterize the impulse sensitivity function (ISF) of a periodic circuit via periodic AC (PAC) analysis. The paper extends the application of ISF from oscillators to other periodic circuits including flip-flops, latches, clocked comparators, and regenerative amplifiers, in order to characterize their important characteristics such as set-up and hold times, regeneration gain, metastability probability, and sampling aperture/bandwidth. Recognizing that the generalized ISF is a subset of a time-varying impulse response, the ISF is efficiently computed based on periodic time-varying system analysis techniques. Compared to the previous ISF characterization method based on transient simulations, a speed-up of ~5× is achieved.

Categories and Subject Descriptors
B.7.2 [**Integrated Circuits**]: Design Aids – *Simulation*

General Terms
Design, Algorithms

Keywords
Simulation, periodic AC analysis, impulse sensitivity function

I. INTRODUCTION

Impulse sensitivity function (ISF) was first used by Hajimiri and Lee [1,2] to analyze the phase noise characteristics of oscillators. They noted that the clock phase of an oscillator is most susceptible to external perturbations when the clock waveform is in transition and least susceptible at the peaks. The ISF of an oscillator was used to describe such time-dependent sensitivity of the oscillator phase to perturbations such as device and supply noises. Based on the ISF and time-varying profile of the noise, Hajimiri and Lee were able to explain why some oscillators like Colpitts oscillators have superior phase noise to ring oscillators. They were also able to explain how the 1/f-flicker noise is up-converted to the oscillation frequency band, based on the periodically time-varying nature of the ISF.

While it was originally intended for oscillators, the concept of ISF can also be extended to other periodic circuits such as periodic samplers. And the ISFs for those circuits carry as important implications as it does for oscillators. Figure 1 describes the ISF of a periodic sampler. If we define the ISF of the sampler as the sensitivity of its final output voltage to the impulse arriving at its input at different times, the ISF essentially describes the aperture of the sampler. An ideal sampler would have the perfect aperture, i.e. sampling the input voltage at exactly one point in time; thus, its ISF would be a Dirac delta function, $\delta(t-t_s)$, where t_s is when sampling occurs. A realistic sampler would rather capture a weighted-average of the input voltage over a certain time window. This weighting function is called the sampling aperture and is equivalent to the ISF. On the other hand, the Fourier transform of the ISF expresses how fast a signal the sampler can track and capture, i.e., the sampling bandwidth, as illustrated in Figure 1(b). Various sample-and-hold and track-and-hold circuits used in analog and data-conversion systems can utilize ISFs to characterize their sampling apertures and bandwidths [3].

The ISF of a periodic sampler has the broader applications than it

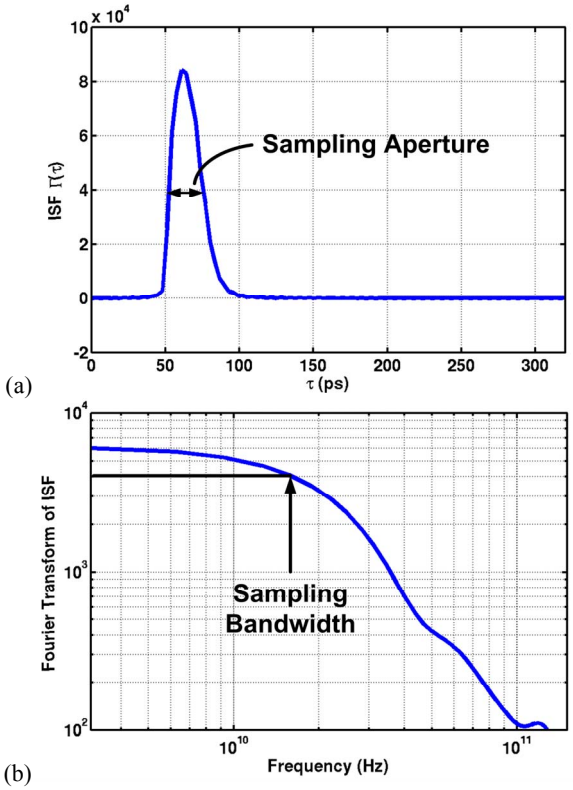

FIGURE 1. Impulse sensitivity function (ISF) of a periodic sampler (a) and its Fourier transform (b).

ICCAD 2008, November 10-13, 2008, San Jose, CA.

may seem. Latches and flip-flops in digital systems, sense-amplifiers in memories, clocked comparators in A/D converters, and regenerative amplifiers in high-speed I/O receivers can all be classified as periodic samplers since they all essentially sample the input voltage at some time points marked by periodic clocks. A minor difference with sample-and-hold circuits is that they may have additional gains due to regeneration, but these gains can be readily expressed by the ISF with its magnitude. In fact, many of the important characteristics of the circuits listed above can be captured by their ISFs. For example, the ISF for a flip-flop can quantify the setup and hold times by the beginning and end of the ISF window. The total area under the ISF corresponds to the effective regenerative gain of the flip-flop, from which one can derive the mean-time-between-failures (MTBF) of a flip-flop-based synchronizer [5].

Recognizing the importance of characterizing ISFs in periodic samplers as well as in oscillators, this paper describes an efficient method to measure the ISFs of periodic circuits via periodic AC (PAC) analysis, which is available from RF circuit simulators such as SpectreRF and ADS.

The only way known to date for characterizing ISFs is to use transient analysis as described in [1,2] for oscillators and [5] for periodic samplers. For example, Hajimiri and Lee applied pseudo impulses to the oscillator at different times and recorded the resulting shifts in the oscillator clock phase. In addition to being very time consuming, measuring ISFs with transient simulation is prone to numerical errors. On one hand, the pseudo impulses must be kept sufficiently small in order not to excite the nonlinear responses of the circuits, which is not a trivial task when the comparator's regeneration time is long and the effective gain is extremely high. On the other hand, simulating the effects of tiny impulses on large-signal waveforms is likely to suffer from numerical inaccuracies. Demir, et al. [6,7] defined perturbation projection vector (PPV) for analyzing phase noise of oscillators. Some of its similarities with the ISF have been noted, although the originators of the ISF and the PPV seem to disagree [8]. While the PPV can be more efficiently simulated via linear periodically time-varying analysis [4], it is not obvious how the definition of the PPV, being the projection vector corresponding to a Floquet multiplier of 1, can be extended to other periodic circuits like samplers which are not autonomous and thus do not have a Floquet multiplier equal to 1.

The method proposed in this paper utilizes the efficient periodic AC simulation [9-12] and the periodic time-varying analysis [13,14] to characterize the ISF, noting that the generalized ISF is in fact a subset of a so-called time-varying impulse response. A time-varying impulse response $\mathbf{h(t, \tau)}$ is defined as the circuit response at time $\mathbf{t}$ responding to an impulse arriving at time τ [13]. In general, the ISF can be regarded as the time-varying impulse response evaluated at one particular observation time $\mathbf{t=t_0}$. For example, the ISF for an oscillator is equivalent to $\mathbf{h_\phi(\infty, \tau)}$, that is, the final response in the oscillator phase to the impulse arriving at time τ. Similarly, the ISF for a periodic sampler is equal to $\mathbf{h(t_0, \tau)}$, where $\mathbf{t_0}$ is the time position of the final output value (e.g. the output voltage immediately before the sampler resets or starts tracking the input again). The proposed method is much more efficient than the transient based ISF characterization and far less prone to numerical inaccuracies.

This paper is organized as follows. First, it briefly reviews the linear time-varying (LTV) system theory and describes the proposed procedures for ISF characterization. Second, the proposed method is applied to examples of periodic samplers and oscillators and the implications of their simulation results are discussed. Finally, the benchmark results against the transient simulations are presented.

II. LINEAR TIME-VARYING SYSTEM THEORY

This section reviews the linear time-varying (LTV) system theory [13,14] and summarizes some key equations governing the input and output of an LTV system.

A linear, time-varying system is a dynamical system for which the superposition principle holds but the time-invariant property may not. That is, if $\mathbf{y_1(t)}$ and $\mathbf{y_2(t)}$ are the responses of the system to the input stimuli $\mathbf{x_1(t)}$ and $\mathbf{x_2(t)}$, respectively, then the response to a linearly combined input $\mathbf{a \cdot x_1(t)+b \cdot x_2(t)}$ is equal to the linearly combined output $\mathbf{a \cdot y_1(t)+b \cdot y_2(t)}$ where $\mathbf{a}$ and $\mathbf{b}$ are real numbers. However, the response to a time-shifted input $\mathbf{x_1(t-t_0)}$ may not be equal to the time-shifted output $\mathbf{y_1(t-t_0)}$.

For such an LTV system, one can define a time-varying impulse response, $\mathbf{h(t, \tau)}$, which describes the system response at time $\mathbf{t}$ to an impulse arriving at time τ. Then the system output $\mathbf{y(t)}$ is related to the input $\mathbf{x(t)}$ as:

$$\mathbf{y(t) = \int_{-\infty}^{\infty} h(t,\tau) \cdot x(\tau) d\tau}\,, \tag{1}$$

Note that in a linear time-invariant (LTI) system, $\mathbf{h(t, \tau) = h(t-\tau)}$ and the above equation reduces to a convolution.

As with LTI systems, an LTV system can be expressed in frequency domain. If $\mathbf{X(j\omega)}$ is the Fourier transform of the input signal $\mathbf{x(t)}$, i.e.,

$$\mathbf{X(j\omega) = \int_{-\infty}^{\infty} x(t) \cdot \exp(-j\omega t) \cdot dt} \quad \text{and} \tag{2}$$

$$\mathbf{x(t) = \frac{1}{2\pi} \int_{-\infty}^{\infty} X(j\omega) \cdot \exp(j\omega t) \cdot d\omega}\,, \tag{3}$$

then substituting EQ(2) in EQ(1) yields:

$$\begin{aligned} \mathbf{y(t)} &= \mathbf{\int_{-\infty}^{\infty} h(t,\tau) \left[\frac{1}{2\pi} \int_{-\infty}^{\infty} X(j\omega) \cdot \exp(j\omega\tau) d\omega \right] \cdot d\tau} \\ &= \mathbf{\frac{1}{2\pi} \int_{-\infty}^{\infty} X(j\omega) \left[\int_{-\infty}^{\infty} h(t,\tau) \cdot \exp(j\omega\tau) d\tau \right] \cdot d\omega} \end{aligned}\,. \tag{4}$$

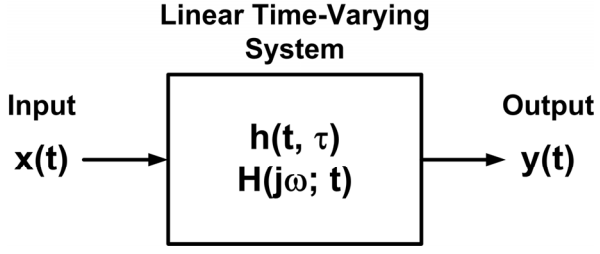

FIGURE 2. Linear time-varying system.

The time-varying transfer function **H(jω; t)** is defined as the Fourier transform of the time-varying impulse response [13], that is:

$$\mathbf{H(j\omega;t)} = \int_{-\infty}^{\infty} \mathbf{h(t,\tau)} \cdot \mathbf{exp(-j\omega(t-\tau))} \cdot \mathbf{d\tau} \,. \qquad (5)$$

For LTI systems, **h(t,τ)=h(t-τ)** and the above expression reduces to that of the time-invariant transfer function, **H(jω)**.

Finally, EQ(4) can be rewritten in terms of **H(jω; t)**:

$$\mathbf{y(t)} = \frac{1}{2\pi} \int_{-\infty}^{\infty} \mathbf{X(j\omega)} \cdot \mathbf{H(j\omega;t)} \cdot \mathbf{exp(j\omega t)} \cdot \mathbf{d\omega} \,. \qquad (6)$$

And it follows that:

$$\mathbf{Y(j\omega) = H(j\omega;\, t) \cdot X(j\omega)}. \qquad (7)$$

For example, if the input is a single-tone sinusoid, $\mathbf{x(t)=exp(j\omega_0 t)}$, then the output **y(t)** is $\mathbf{H(j\omega_0;\, t)\cdot exp(j\omega_0 t)}$. For linear, periodically time-varying (LPTV) systems, **h(t, τ) = h(t+T, τ+T)** and **H(jω; t) = H(jω; t+T)** where **T** is the period of the time-varying dynamics of the system.

III. CHARACTERIZING IMPULSE SENSITIVITY FUNCTION VIA PERIODIC AC ANALYSIS

As mentioned earlier, the impulse sensitivity function (ISF), denoted as **Γ(τ)**, is essentially a time-varying impulse response evaluated at one particular time point $\mathbf{t=t_0}$. In other words, $\mathbf{\Gamma(\tau) = h(t_0,\, \tau)}$. For oscillators, the ISF expresses the amount of final phase shift caused by the impulse arriving at time **τ**; thus $\mathbf{t_0}$ is ∞. For periodic samplers, $\mathbf{t_0}$ is of finite value because a sampler resets its previously sampled value before sampling the next one. Hence, the sampler's output does not accumulate all the past input contributions like oscillators. Therefore, the reasonable choice of $\mathbf{t_0}$ for samplers would be the time immediately before the sampler resets when the sampled value takes the full effect at the output.

The periodic AC analysis from many RF circuit simulators like spectreRF computes not just one, but a series of transfer functions targeted at various harmonic sidebands.[1] It is because in an LPTV system, a sinusoidal excitation at a frequency **ω** can give rise to multiple sinusoidal responses at frequencies of $\mathbf{m\cdot\omega_c+\omega}$, where **m** is an integer and $\mathbf{\omega_c}$ is the fundamental frequency of the periodic system ($\mathbf{\omega_c=2\pi/T}$). This is in contrast to LTI systems, where the response to a sinusoid is always a sinusoid at the same frequency. We will use $\mathbf{H_m(j\omega)}$ to represent the frequency response of the system at the m-th harmonic output sideband to a unit **jω**-sinusoid.

These sideband transfer functions $\mathbf{H_m(j\omega)}$ are basically the Fourier coefficients of the time-varying transfer function **H(jω; t)**. Since **H(jω; t)** is periodic in **T**, i.e., **H(jω; t)** = **H(jω; t+T)**, it can be expressed in a Fourier series:

$$\mathbf{H(j\omega;t)} = \sum_{m=-\infty}^{\infty} \mathbf{H_m(j\omega)} \cdot \mathbf{exp(jm\omega_c t)} \,. \qquad (8)$$

[1] It has come to our knowledge that SpectreRF calculates H(jω;t) internally first and derives $H_m(j\omega)$ via Fourier series expansion [15]. While the simulator has an option to report H(jω;t) directly (`outputperiod`), it reports only the real values.

The next step is to derive the time-varying impulse response from **H(jω; t)**. However, it is not always feasible to compute the direct inverse Fourier transform on **H(jω; t)** to recover **h(t, τ)** (e.g. consider **H(jω)=1/jω**). Instead, we compute the response to a periodic impulse train, that is:

$$\mathbf{x(t)} = \sum_{n=-\infty}^{\infty} \mathbf{\delta(t-\tau-nkT)} \,, \qquad (9)$$

where **δ(·)** is a Dirac delta function and the period of the impulse train is a integer multiple of the system period, **kT**. The idea is that if the impulse response of the system settles to zero long before the next impulse arrives, then the system response to this impulse train would be approximately equal to the periodic repetition of the true impulse response, i.e.:

$$\mathbf{y(t)} \cong \sum_{n=-\infty}^{\infty} \mathbf{h(t,\tau+nkT)} \,, \qquad (10)$$

and **y(t)** would be approximately equal to **h(t, τ)** for $\mathbf{\tau \le t < \tau+kT}$. Note that this assumption is not valid for oscillators whose impulse response does not return to zero but settles to a finite non-zero value. In such cases, one can apply a similar derivation for computing the response to the time-derivative of a periodic impulse train instead (i.e. **jω·X(jω)**). More details will be discussed in Section V.

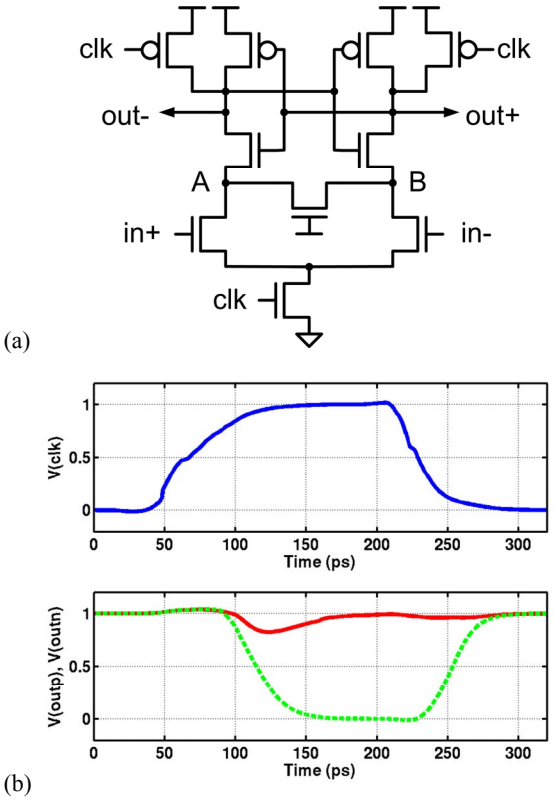

FIGURE 3. (a) Circuit schematics of a StrongARM latch and (b) the waveforms illustrating its operation.

The Fourier transform **X(jω)** of the **kT**-periodic impulse train is:

$$X(j\omega) = \frac{\omega_c}{k} \sum_{n=-\infty}^{\infty} \delta(\omega - n\omega_c / k) \cdot \exp(-j\omega\tau) \qquad (11)$$

where ω_c is $2\pi/T$. Then from EQ(6), the response **y(t)** is:

$$\begin{aligned} y(t) &= \frac{1}{2\pi}\int_{-\infty}^{\infty} H(j\omega;t)\cdot X(j\omega)\cdot e^{j\omega t}\cdot d\omega \\ &= \frac{1}{kT}\sum_{n=-\infty}^{\infty} H(jn\omega_c / k;t)\cdot e^{jn\omega_c / k\cdot(t-\tau)} \end{aligned} \qquad (12)$$

Substituting EQ(8) in EQ(12) yields the expression for the approximate time-varying impulse response:

$$\begin{aligned} h(t,\tau) &\cong y(t) \\ &= \frac{1}{kT}\sum_{n=-\infty}^{\infty}\sum_{m=-\infty}^{\infty} H_m(jn\omega_c / k)\cdot e^{jm\omega_c t + jn\omega_c / k\cdot(t-\tau)} \end{aligned} \qquad (13)$$

for $\tau \le t < \tau + kT$ and $h(t, \tau) = 0$ elsewhere.

Finally, the ISF $\Gamma(\tau)$ is equal to $h(t, \tau)$ when $t = t_0$ if $t_0 > \tau$:

$$\Gamma(\tau) \cong \frac{1}{kT}\sum_{n=-\infty}^{\infty}\sum_{m=-\infty}^{\infty} H_m(jn\omega_c / k)\cdot e^{jm\omega_c t_0 + jn\omega_c / k\cdot(t_0-\tau)} \qquad (14)$$

In practice, the summations are carried out over finite ranges of **n** and **m**, for example, -50~50. For each combination of **n** and **m**, the PAC analysis needs to be performed to compute $H_m(jn\omega_c/k)$, the m-th harmonic response to the excitation at $n\omega_c/k$.

The next two sections will describe more specific details about computing ISFs for periodic samplers and oscillators.

IV. ISF ANALYSIS OF PERIODIC SAMPLERS

This section demonstrates the simulation of the ISF for a periodic sampler shown in Figure 3(a). This sampler is commonly called a StrongARM latch, because this latch circuit followed by an RS-latch was used as a flip-flop element in the DEC StrongARM processor in 1996 [16]. Because of its high sampling bandwidth and low static power consumption, the same circuit topology is also found in many A/D converters and high-speed I/O receivers [17].

The waveforms in Figure 3(b) illustrate the operation of the StrongARM latch. Initially, when the clock signal **clk** is low, the input pair is deactivated and the output voltages are precharged to **Vdd**. When the clock switches from low to high, the input pair starts discharging the internal nodes **A** and **B** as a function of the input voltages, **in+** and **in-**. Once sufficient amount of voltage difference is developed across the nodes **A** and **B**, the cross-coupled inverter pair starts amplifying the voltage difference via positive feedback (regeneration). When the clock returns to low, the outputs are precharged back to **Vdd** and the latch prepares itself for the next cycle. Hence, the StrongARM latch essentially samples the input voltage shortly after the clock rises and amplifies it with a large gain.

The detailed procedure for characterizing the ISF of this sampler is outlined as follows. First, apply the proper input voltages that place the sampler in a metastable state and perform the periodic steady-state (PSS) analysis. Second, perform the PAC analysis. Third, based on the simulated PAC response, pick a time point t_0 at which the ISF is to be computed and derive the ISF according to EQ(14).

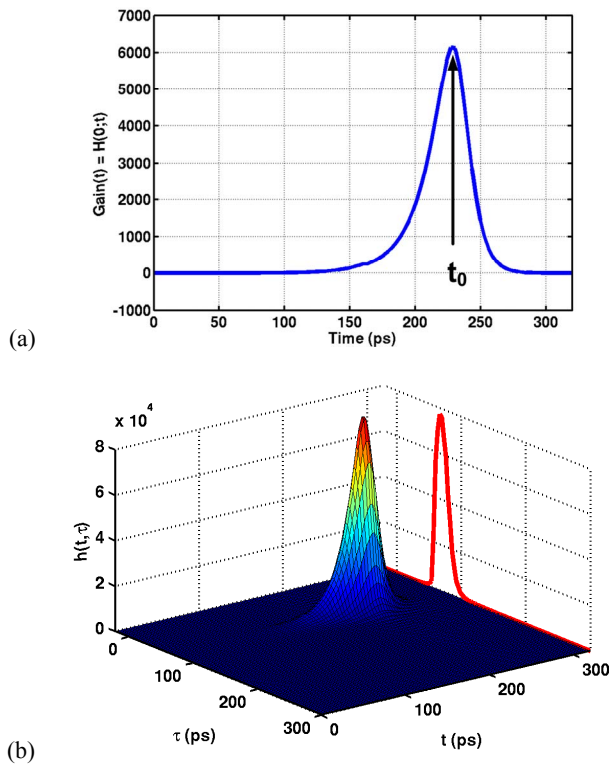

FIGURE 4. (a) Time-varying gain and (b) time-varying impulse response of the periodic sampler.

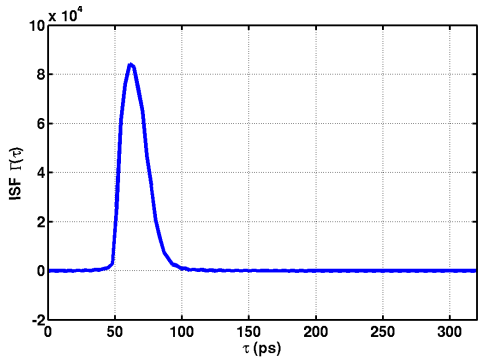

FIGURE 5. Simulated ISF of the StrongARM latch.

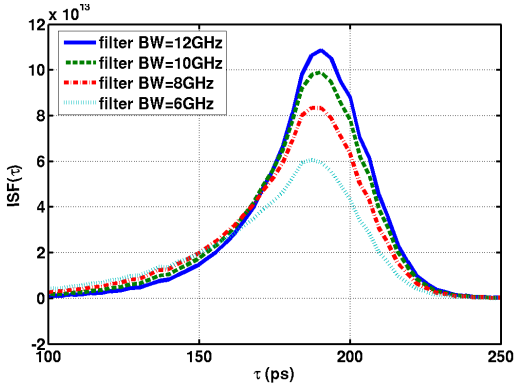

FIGURE 6. Influence of a preceding low-pass filter on the sampler aperture.

One possible candidate for the ISF measurement point $\mathbf{t_0}$ is the time at which the output voltage is amplified to the largest value. Figure 4(a) plots the PAC response of the sampler to a small-signal DC input, that is, the time-varying transfer function evaluated at ω=0. This response, $\mathbf{H(0; t)}$, can be calculated from the sideband transfer functions $\mathbf{H_m(0)}$:

$$\mathbf{H(0;t) = \sum_{m=-\infty}^{\infty} H_m(0) \cdot \exp(jm\omega_c t)} \,. \qquad (15)$$

Figure 4(b) plots the time-varying impulse response of the sampler, $\mathbf{h(t, \tau)}$. This 3-D plot illustrates how the ISF, the cross-section perpendicular to the **t**-axis, changes with the selection of $\mathbf{t_0}$.

Figure 5 plots the simulated ISF of the StrongARM latch for the chosen $\mathbf{t_0}$. With respect to the clock edge, the peak of the ISF is located 26ps later, which marks the time when the effective sampling occurs. The total area under the ISF is the sampling gain, which is equal to the time-varying gain in Figure 4(a) measured at $\mathbf{t_0}$. The width of the ISF pulse corresponds to the aperture width. The narrower the aperture width is, the more sensitive the sampler is to the fast-changing input signal. For flip-flops, the width of the ISF corresponds to the setup and hold time window of a flip-flop, also referred to as uncertainty window or forbidden zone, because the outcome is uncertain if the input changes within that time window.

Samplers are often preceded by additional circuits that may filter some frequency contents. For example, there may be a pre-amplifying stage before a clocked comparator to offer isolation or additional gain to drive the input load of the sampler. When the

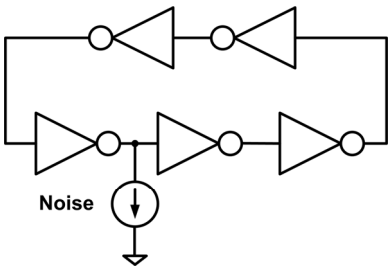

FIGURE 7. An example inverter-based ring oscillator. The current noise injection point is indicated.

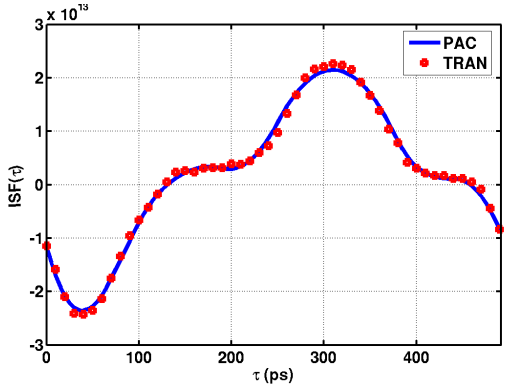

FIGURE 8. Simulated ISF of the ring oscillator. The plot shows both the results from the proposed PAC analysis and the transient analysis.

preceding stage is a low-pass filter, the effective sampling aperture becomes wider. In expressions, the effective ISF $\mathbf{\Gamma_{eff}(\tau)}$ including the preceding linear filter impulse response $\mathbf{h_{filter}(t)}$ is:

$$\mathbf{h_{eff}(t,\tau) = \int_{-\infty}^{\infty} h_{filter}(s) \cdot h(t, \tau + s) \cdot ds} \,, \qquad (16)$$

$$\mathbf{\Gamma_{eff}(\tau) = h_{eff}(t_0, \tau) = \int_{-\infty}^{\infty} h_{filter}(s) \cdot \Gamma(\tau + s) \cdot ds} \,. \qquad (17)$$

Figure 6 plots the simulated effective ISFs of the StrongARM sampler preceded by a first-order RC low-pass filter with various cut-off frequencies. It is observed that the low-pass filter increases the sensitivities at the earlier part of the ISF, thus widening the sampling aperture. For flip-flops and latches, one can make a similar observation that a high-fanout buffer preceding the flip-flop or latch increases the set-up time. On the other hand, it can be shown that the loading at the output of the regenerative sampler slows down the regeneration and widens the sampling aperture at the later part of ISF, or equivalently, increasing the hold time. Therefore, based on the shape of the ISF, one can tell whether the sampling bandwidth is being limited by the input loading or by the output loading of the sampler. Hence, the ISF provides many insights as to how to improve the circuit performance.

V. ISF ANALYSIS OF OSCILLATORS

The ISFs for oscillators are useful guides for circuit designers in achieving low phase noise, even when the phase noise itself can be simulated more conveniently and accurately with periodic NOISE analysis [6]. For example, Hajimiri and Lee [1,2] asserted that in order to suppress 1/f-noise up-conversion from a particular noise source, the ISF with respect to the noise source must have a zero DC value over the period. Also, they claimed that in order to achieve low phase noise, the rms value of the ISF must be minimized. The ISF offers good design insights, which has led designers to invent better oscillator topologies. For example, Hajimiri and Lee proposed the differential LC oscillator with both nMOS and pMOS active regenerators [18], aiming to make rise and fall transitions symmetric and the DC value of the ISF close to zero. Shaeffer and Kudszus [19] coupled two oscillators to purposely misalign the peak points of the ISF and device noise profile so that the effective noise contribution is minimized.

Figure 7 shows a simple inverter-based ring oscillator to demonstrate our proposed method of computing the ISF. A current noise source at one of the ring oscillator node is considered.

Procedures for characterizing the ISFs for oscillators are slightly different from those described earlier in Section III, because the impulse response of the oscillator phase does not return to zero and the approximation with the periodic impulse response cannot apply. Instead, we can apply a similar approximation to the response to the time-derivative of the periodic impulse response since the time-derivative of the impulse response does return to zero. The time-derivative of the periodic impulse response, $\mathbf{y'(t)}$, can be expressed as:

$$\mathbf{y'(t) = \frac{1}{2\pi} \int_{-\infty}^{\infty} H(j\omega; t) \cdot j\omega X(j\omega) \cdot e^{j\omega t} \cdot d\omega}$$
$$\mathbf{= \frac{1}{kT} \sum_{n=-\infty}^{\infty} \sum_{m=-\infty}^{\infty} \frac{jn\omega_c}{k} \cdot H_m(jn\omega_c / k) \cdot e^{jm\omega_c t + jn\omega_c (t-\tau)/k}} \qquad (18)$$

where the sideband transfer function $\mathbf{H_m(jn\omega_c/k)}$ is evaluated at a small offset $\mathbf{\Delta\omega}$ from $\mathbf{n\omega_c/k}$ rather than at $\mathbf{n\omega_c/k}$ because $\mathbf{H_m(\cdot)}$ for oscillators may have infinite values at those frequencies.

The ISF of the oscillator, $\mathbf{\Gamma_{osc}(\tau)}$, is then computed as:

$$\Gamma_{osc}(\tau) = h_\phi(\infty,\tau) = \int_\tau^{\tau+kT} y'(t)\cdot dt = \lim_{\Delta\omega\to 0}\frac{1}{kT}\sum_{n=-\infty}^{\infty}\sum_{m=-\infty}^{\infty} K_{n,m,\Delta\omega}\cdot H_m(jn\omega_c/k + j\Delta\omega) \quad (19)$$

where $\mathbf{K_{n,m,\Delta\omega}}$ is:

$$K_{n,m,\Delta\omega} = \frac{n/k + \Delta\omega/\omega_c}{m + n/k + \Delta\omega/\omega_c}\cdot e^{jm\omega_c\tau}\left[e^{j(m\omega_c + n\omega_c/k + \Delta\omega)kT} - 1\right].$$

Figure 8 plots the ISFs measured by the described method using PAC analysis and the previous method using transient analysis [1,2]. They are in good agreement, validating the correctness of our methodology.

Table I summarizes the simulation times for the test cases described in this paper. The simulations were run with SpectreRF on a 3.6GHz Intel Xeon processor machine with 4GB of main memory. For both cases of computing ring oscillator ISF and sampler ISF, the proposed method achieved speed-ups of ~5× compared to the transient-based method.

VI. CONCLUSIONS

This paper extended the use of impulse sensitivity functions to a broader application, including that of periodic samplers such as flip-flops, latches, and comparators. We demonstrated that the ISFs for samplers can characterize many important characteristics of the circuits, including the setup and hold times, regenerative gain, metastability probability, and sampling aperture/bandwidth.

The ISF can be efficiently simulated by recognizing that the ISF is a subset of time-varying impulse response and utilizing the periodic AC simulation and the linear time-varying system analysis. This paper demonstrated the validity and efficiency of the proposed ISF characterization method with the examples of a periodic sampler and an oscillator.

VII. REFERENCES

[1] A. Hajimiri and T. H. Lee, "A General Theory of Phase Noise in Electrical Oscillators," IEEE J. Solid-State Circuits, Feb. 1998, pp. 179-194.

[2] T. H. Lee and A. Hajimiri, "Oscillator Phase Noise: A Tutorial," IEEE J. Solid-State Circuits, Mar. 2000, pp. 326-336.

[3] H. Johansson and C. Svensson, "Time Resolution of NMOS Sampling Switches Used on Low-Swing Signals," IEEE J. Solid-State Circuits, Feb. 1998, pp. 237-245.

[4] C. L. Portmann and T. H. Meng, "Supply Noise and CMOS Synchronization Errors," IEEE J. Solid-State Circuits, Sep. 1995, pp. 1015-1018.

[5] T. Toifl, et al., "A 22-Gb/s PAM-4 Receiver in 90-nm CMOS SOI Technology," IEEE J. Solid-State Circuits, Apr. 2006, pp. 954-965.

[6] A. Demir, A. Mehrotra, and J. Roychowdhury, "Phase Noise in Oscillators: A Unifying Theory and Numerical Methods for Characterization," IEEE Trans. Circuits and Systems – I: Fund. Th. Appl., May 2000, pp. 655-674.

[7] A. Demir and J. Roychowdhury, "A Reliable and Efficient Procedure for Oscillator PPV Computation, With Phase Noise Macromodeling Applications," IEEE Trans. on Computer-Aided Design and Integrated Circuits and Systems, Feb. 2003, pp. 188-197.

[8] A. Demir and J. Roychowdhury, "On the Validity of Orthogonally Decomposed Perturbations in Phase Noise Analysis," Bell Labs., Murray Hill, NJ, Tech. Memo., 1997.

[9] K. S. Kundert, "Introduction to RF Simulation and Its Application," J. Solid-State Circuits, Sept. 1999, pp. 1298-1319.

[10] M. Okumura, T. Sugawara, and H. Tanimoto, "An Efficient Small Signal Frequency Analysis Method of Nonlinear Circuits with Two Frequency Excitations," IEEE Trans. Computer-Aided Design of Integrated Circuits and Systems, Mar. 1990, pp. 225-235.

[11] R. Telichevesky, K. Kundert, and J. White, "Receiver Characterization Using Periodic Small-Signal Analysis," In Proc. IEEE Custom Integrated Circuits Conf., May 1996, pp. 449-452.

[12] R. Telichevesky, K. S. Kundert, J. K. White, "Efficient AC and Noise Analysis of Two-Tone RF Circuits," in Proc. ACM/IEEE Design Automation Conf., June 1996, pp. 292-297.

[13] L. Zadeh, "Frequency Analysis of Variable Networks," Proc. I.R.E., Mar. 1950, pp. 291-299.

[14] J. Roychowdhury, "Reduced-Order Modeling of Time-Varying Systems," IEEE Trans. on Circuits and Systems—II: Analog and Digital Signal Processing, Oct. 1999, pp. 1273-1288.

[15] J. R. Phillips, *Personal Communication*, Aug. 2007.

[16] J. Montanaro, et al., "A 160MHz, 32b, 0.5W CMOS RISC Microprocessor," IEEE J. Solid-State Circuits, Nov. 1996, pp. 1703-1714.

[17] M.-J. E. Lee, W. J. Dally, and P. Chiang, "Low-Power Area-Efficient High-Speed I/O Circuit Techniques," IEEE J. Solid-State Circuits, Nov. 2000, pp. 1591-1599.

[18] A. Hajimiri and T. H. Lee, "Design Issues in CMOS Differential LC Oscillators," IEEE J. Solid-State Circuits, May 1999, pp. 717-724.

[19] D. K. Shaeffer and S. Kudszus, "Performance-Optimized Microstrip Coupled VCOs for 40-GHz and 43-GHz OC-768 Optical Transmission," IEEE J. Solid-State Circuits, vol. 38, no. 7, July 2003, pp. 1130-1138.

Test Case	Proposed PAC-based ISF Simulation	Transient-based ISF Simulation
VCO	52 sec	256 sec
Sampler	48 sec	225 sec

TABLE I. ISF simulation benchmark summary.